International Symposium
On Turbulence and Shear Flow
Phenomena (TSFP-8)
August 28 - 30, 2013 Poitiers, France

PIV CHARACTERISATION OF A FLOW SEPARATION INDUCED BY A 22° FLAP

C. Cuvier[1,2,4], **J.M. Foucaut**[1,2], **C. Braud**[1,3], **M. Stanislas**[1,2]
Univ Lille Nord de France[1] F-59000 Lille, EC Lille[2], CNRS[3], ENSAM[4],
Laboratoire de Mécanique de Lille (UMR 8107)
Boulevard Paul Langevin,
59655 Villeneuve d'Ascq Cédex, France.
christophe.cuvier@gmail.com

ABSTRACT

The flow separation induced by a flap of a two dimensional ramp has been characterized through a streamwise 2D2C PIV measurement at mid-span. The field of view follows the wall surface and its size is about 28.7 cm in height above the wall and the curvilinear length is about 94 cm, so that it contains all the separation bubble and a part of the flow upstream and downstream of it. Four 2k*2k cameras where used to keep a relatively good spatial resolution. The incoming boundary layer thickness upstream the separation is about 19 cm and it momentum Reynolds number about 10000. The separation border was detected with the backflow coefficient and it results that the separation length is about 61 cm and the maximum height about 3 cm. The Reynolds stresses and their main production terms were also determined. It results that a region of high turbulence intensity develops above the separation border for all the measured components. The production of $\overline{u'^2}$ dominates the production for turbulent kinetic energy which imposes a redistribution from $\overline{u'^2}$ to $\overline{v'^2}$ to explain the increase of the last one. The production term $\overline{u'^2}\frac{\partial U}{\partial x}$ drives the production of $\overline{u'^2}$ in the first part of the flap which is not the case for zero pressure gradient boundary layers. Finally a high similarity is observed between $\overline{v'^2}$ and $\overline{u'v'}$ as the production of the last one is dominated by $\overline{v'^2}\frac{\partial U}{\partial y}$.

Key words : Turbulent boundary layers, 2D2C PIV, flow separation.

INTRODUCTION

Flow separation induced by a strong adverse pressure gradient is often encountered in turbomachinery and aircraft applications and leads to a drop in efficiency. Trying to understand the mechanisms that cause flow detachment is then an important challenge. Simpson (1989) defined several steps in the separation process based on the backflow coefficient χ, which is defined as the ratio of the time where the flow is reversed (i.e. opposite to local streamwise direction), over the total time. The first one is Incipient Detachment (ID), defined by $\chi \simeq 1\%$. It characterises flow with rare backflow occurrences. The second one is Intermittent Transitory Detachment (ITD) characterized by $\chi \simeq 20\%$. The third one is Transitory Detachment (TD) defined by $\chi \simeq 50\%$ and the last one is Detachment (D), defined by the mean wall shear stress equal to 0 (i.e. $\overline{\tau_w} = 0$).

He defined also the mean separation point by either D or TD events, even if the first one is mostly used. In most experiments, the two criteria give the same positions. D and TD are equivalent only if the probability density function of the streamwise velocity is symmetric at the separation point. In the same way, the mean reattachment point can also be defined with D or TD events. For flow where strong APG leads to separation, positions of the instantaneous separation and reattachment points fluctuate around the mean separation point and the mean reattachment point respectively (Simpson (1989)), so the flow can be affected largely upstream and downstream of them. However, for an "imposed separation" (backward facing step for example), the separation point is fixed and only the instantaneous reattachment point position fluctuate around the mean one. By analogy, the border of the mean separation bubble can be defined either by $\chi = 50\%$ or $U = 0$, with U the mean streamwise velocity. The mean separation bubble is then defined either by $\chi \geq 50\%$ or $U \leq 0$.

Separation criterion based on the shape factor H have also been developed. For Dengel & Fernholz (1990), the beginning of the separation is characterized by a shape factor above 2.85 ± 0.1. However, Mellor & Gibson (1966) suggested a limit value of 2.35 and Bradshaw (1967) suggested a limit value of 2.5 ± 0.1, so this kind of criterion seems to be not reliable. High values of the shape factor are characteristic of weak boundary layers, but the separation point can not be located reliably with H (Angele (2003)).

In the 80's, Simpson and co-authors (Simpson *et al.* (1977, 1981*a*,*b*), Chehroudi & Simpson (1985)) have done an intensive work on a flow separation on a flat plate induced by an adjustable diverging wind-tunnel top wall, which is still today the reference. In the separated region, they used laser Doppler anemometry for flow diagnostic and hot-wire anemometry outside the bubble border. They provided mean velocity, turbulent intensity and production profiles (U, V, $\overline{u'^2}$, $\overline{v'^2}$, $\overline{u'v'}$, $-\overline{u'^2}\frac{\partial U}{\partial x}$ and $-\overline{u'v'}\frac{\partial U}{\partial y}$) at different streamwise stations in the separated region. These detail experiments have brought a lot of information about the turbulence organisation of a flow separation. Especially, they have exhibited a region of high turbulence which develops above the bubble border. This region is also characterised by high turbulence production which dominates the production inside the separated region. The results of these studies are summarized and actualized in Simpson (1989).

On a smoothly contoured ramp, Song *et al.* (2000) performed a characterisation of a flow separation with the same methodology as Simpson and co-authors. They obtained similar results, indicating that the turbulence organisation of a flow separation seems to be not too much affected by what caused the detachment (adverse pressure gradient or curvature). Song & Eaton (2004) have completed the experiment by a streamwise PIV analysis above the separation border. However, the separation region was not inside the PIV field, which is problematic for understanding the flow separation mechanisms and the interaction between the reverse flow and the external flow.

In the present study a separated flow induced by a 22° flap is characterised in detail with a streamwise two components (2C) PIV measurement which includes all the separated region. The aim is to give a detailed description of the turbulence organisation of this flow, including some relevant turbulence production terms.

THE EXPERIMENT

The wind tunnel facility and the ramp

The experiments were conducted in the LML boundary layer wind tunnel at $U_\infty = 10$ m/s (see Figure 1). A boundary layer develops on the 20 m long lower wall to reach around 30 cm at the end. This thick boundary layer allows good spatial resolution. The test section is 2 m span and 1 m height and the free-stream velocity is ranging from 3 to 10 m/s ($\pm 0.5\%$). In this experiment, the wind tunnel was used in closed-loop configuration to allow temperature regulation ($\pm 0.2°C$). For detailed characteristics of the wind tunnel, see Carlier & Stanislas (2005).

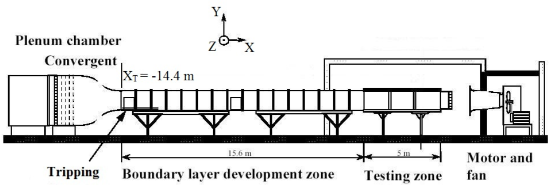

Figure 1. Schematic view of the LML wind tunnel

The ramp model was mounted on the wind tunnel floor such as the beginning of the ramp was 14.4 m downstream of the entrance of the test section. Figure 2 gives a schematic view of the ramp. It is composed of four parts. The first one is a smooth converging part with a contraction ratio of 0.75. The second part is an articulated flat plate of more than 2 m. The angle between this plate and the wind tunnel floor is called α and is counted positive if it corresponds to a positive rotation around the z axis (Figure 2). The angle α tunes the pressure gradient of the boundary layer that develops on the 2.1 m flat plate. α is ranging from 2° to $-4°$. The third part of the ramp is an other articulated flat plate (called flap). The angle between this plate and the wind tunnel floor is called β and its sign follows the same convention as α. β is ranging from $-5°$ to $-40°$. The aim of the flap is to allow to create and fix a flow separation. The angle β tunes its strength and its extend. The last part is a flexible plate to allow smooth connection between the end of the flap and the floor of the wind tunnel.

The origin O of the wind tunnel coordinate system that will be used (see Figure 2) is placed at midspan on the lower wall, at the beginning of the converging part of the ramp.

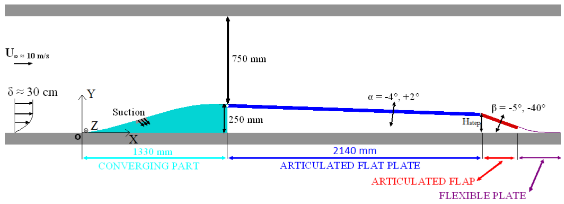

Figure 2. Schematic view of the ramp

The X-axis is along the streamwise direction, the Y-axis is normal to the wall and this reference frame is direct. In order to represent the velocity results along the ramp and in the separation region, a curvilinear abscissa s will be used on the model with the origin at O, and a local Frenet (x, y, z) reference frame with the origin at s, the x-axis tangent to the wall, the y-axis normal and the z-axis spanwise.

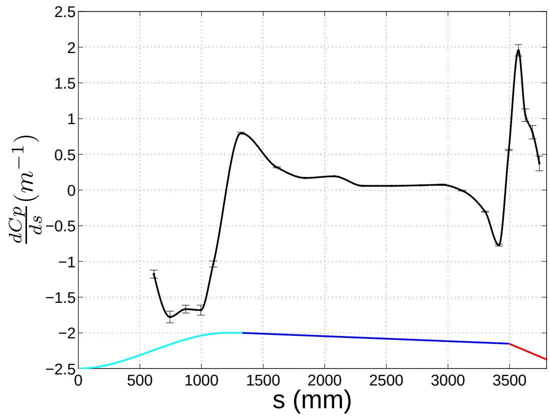

Figure 3. Streamwise pressure gradient distribution for the selected ramp configuration at $U_\infty = 10$ m/s

In the present study, the angles α and β were fixed at respectively $-2°$ and $-22°$. This configuration corresponds to a mild adverse pressure gradient on the flat plate followed by a separation on the flap which remains more or less 2D. This ramp set-up was characterized with wall pressure measurements, oil-film visualisation on the flap and by 5 hot-wire profiles on the flat plate. Details about this characterization can be found in Cuvier (2012). Figure 3 gives the pressure gradient distribution along the ramp and Table 1 gives the main boundary layer parameters. It has to be noted that the separation starts at the flap articulation at $s = 3500$ mm.

Table 1. Boundary layer characteristics for the selected ramp configuration at $U_\infty = 10$ m/s

St	s (mm)	δ (cm)	δ^* (mm)	θ (mm)	Re_θ
St1	1508	17.4	14.4	12.2	10100
St2	1974	19.6	16.5	13.7	10600
St3	2440	20.3	17.9	14.7	11700
St4	2968	21.2	20.3	16.5	12600
St5	3382	19.0	16.4	13.5	10100

St	H	U_e (m/s)	u_τ (m/s)	$(\frac{\partial P}{\partial s})^+$ ($\times 10^3$)	$\beta_{Clauser}$
St1	1.18	12.9	0.482	3.28	1.44
St2	1.21	12.6	0.459	1.47	0.70
St3	1.22	12.5	0.462	0.46	0.24
St4	1.23	12.4	0.435	0.67	0.38
St5	1.21	12.3	0.465	-5.54	-2.56

PIV Experiment

A streamwise 2D2C PIV set-up at mid-span of the ramp and on all the ramp flap was used in the present study (see Figure 4). To obtain a large field which contains all the separation region and a part of the flow upstream and downstream of it, without scarifying the resolution, four synchronized Hamamatsu C9300 cameras of 2048 x 2048 px^2 were used. Between two PIV set-ups, there was a common region in order to obtain a large continuous field from the four set-ups and to obtain the uncertainty as proposed by Kostas *et al.* (2005) and Herpin *et al.* (2008). 50 mm Nikon lenses were placed on the cameras at 1.08 m from the measurement plane. The magnification M was about 0.049. The aperture was set at $f_\# = 5.6$, which allows particle image diameters slightly larger than one pixel (about 1.3 px), which unfortunately increases the uncertainty as it is below the optimum value (Foucaut *et al.* (2003)). The size of the total field is about 28.7 cm in height above the wall and the curvilinear length is about 94 cm (with about 17.5 cm upstream the separation).

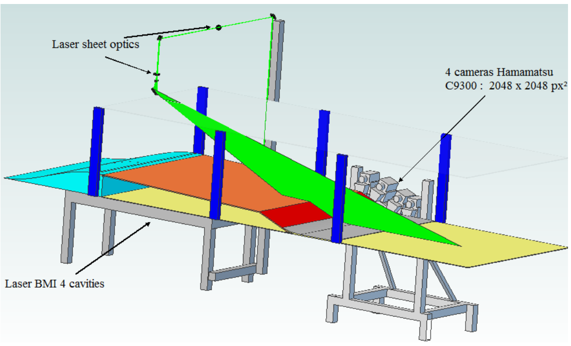

Figure 4. Scheme for the 2D2C PIV set-up used.

A light sheet of about 60 cm wide and 0.8 mm thick in the middle of the field of view was realised with a double pulsed Nd:YAG laser with an energy of 425 mJ per pulse. To minimized the laser reflection on the wall, a special rhodamine paint developed by ONERA (Office National d'études et de Recherches Aérospatiales) was applied on the ramp all along the light sheet position. The paint was applied on a 2 cm wide and 0.18 mm thick black electrical insulation tape to easily renew it. The total thickness of the tape and the rhodamine paint was about 0.25 mm, which corresponds to about 8 wall units before the separation. To filter the rhodamine emission, 50 mm diameter bandpass filters, centred at the laser wave length, were set on the 50 mm Nikon lenses. The time between the two laser pulses was set at $\Delta t = 80\mu s$, so that the out of plane motion was limited, as recommended by Foucaut *et al.* (2003). The free-stream displacements is then of the order of 6 to 7 pixels, which does not optimize the dynamic, as near the recirculation bubble the velocities are largely smaller.

To obtain the velocity in the local reference frame attached to the wall, special software were made to make a special PIV mesh which follows the wall (i.e. each vertical mesh line is normal to the local surface). The mesh and the field of view of each camera are presented in Figure 5 (the meshing procedure is explained in Cuvier (2012)).

The meshes size used was 10×10 pixels^2. The distance from the wall of the first mesh point was 16 pixels to prevent laser reflection to be inside the interrogation win-

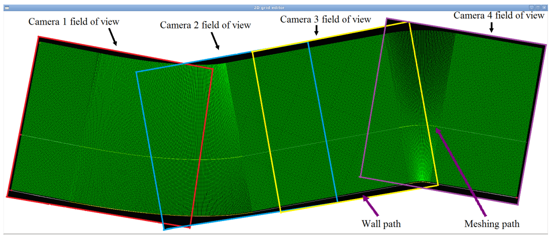

Figure 5. Field of view of each camera and PIV mesh.

dows. This grid was then designed to used 32 x 32 px^2 interrogation windows with a mean overlapping of about 70% (maximum 90% and minimum 35%). The final grid obtained has then 642 points along the wall and 188 points along the wall-normal direction. This leads to a mean grid spacing of 1.5 mm $\times$ 1.5 mm. This corresponds to about 45 wall units, with u_τ taken at $s = 3382$ mm. The first measurement point is at 2.4 mm from the wall which corresponds to about 72 wall units.

The MatPIV.1.6.1 toolbox for Matlab software, written by J. K. Sveen from Oslo University, was modified and used to perform the 2D2C PIV processing on the specific grid. The toolbox was adapted to run on the free software Octave. Four passes were used, a first one with 64 x 64 px^2 interrogation window and three with 32 x 32 px^2. In the final pass, the software used a 1D Gaussian fit based on three points to obtain displacement accuracy below 1 *px*.

As proposed by Kostas *et al.* (2005) and Herpin *et al.* (2008), the total uncertainty on the mean streamwise velocity U is estimated in the merging regions by $\Delta U = \pm(\overline{u_{syst1} - u_{syst2}})$ ($syst1$ and $syst2$ refer to the two cameras). The formula is also valid for V by replacing u by v. The same will be true for the next formulas. The random PIV uncertainty with a 66% confidence index, is estimated by $\sigma_u = \pm(u_{syst1} - u_{syst2})_{RMS}$ for the u component. The PIV random uncertainty gives a positive bias error for the Reynolds stresses. The uncertainty on $\sqrt{\overline{u'^2}}$ is then given by $\frac{1}{2}\Delta\overline{u'^2} = \pm\frac{1}{2}((u_{syst1} - u_{syst2})_{RMS})^2$. For more details about these PIV uncertainties estimation, see Cuvier (2012).

For the present experiment, 5000 uncorrelated fields at 4 Hz were acquired to obtain a convergence on the mean value below $\pm1\%$ and on the turbulence intensity below $\pm4\%$. The total error on the mean velocity components, estimated with the merging regions and normalised by the freestream velocity $U_\infty = 10$ m/s, is below $\pm1\%$ in the freestream region and larger (below $\pm4\%$) near the wall and in the separated region, due to smaller velocities, stronger gradients and out of plane motion. For the random error, in the external region, it is between 0.11 (upstream the corner) and 0.23 pixel (downstream part of the field of view). It is more than two times bigger than the optimum one obtained by Foucaut *et al.* (2003) with synthetic images but it remains acceptable for real PIV measurements. Near the wall and the separation, this uncertainty is increased to reach a value of 0.3 pixel. Finally, the total uncertainty on the turbulence intensity components normalised by the freestream velocity is below $\pm0.8\%$ in the outer flow and $\pm3\%$ near the wall.

RESULTS

Mean velocity and separation border

In order to obtain a better assessment of the near wall flow behaviour, the velocities will be represented only in the local reference frame attached to the wall (x, y, z). U is the velocity parallel to the wall and V the velocity normal to it. Figure 6 shows the mean streamwise velocity distribution normalized by $U_\infty = 10\ m/s$. This component decreases slightly with the streamwise position X due to the section enlargement. Near the wall, before the articulation (at $X = 3.47$ m), when approaching it, higher velocities are observed. This is coherent with the decrease of the boundary layer thickness (δ) observed in this region. This decrease of δ is due to the strong favourable pressure gradient just upstream of the flap articulation as seen in Table 1 and Figure 3. On the flap, a small region of negative streamwise velocities is exhibited which corresponds to the separation. The shear layer is clearly visible and extends rapidly in the wall-normal direction with the streamwise position X. At the end of the field of view, the size of this shear layer is of the order of the flap height (H_{step}, see Figure 2).

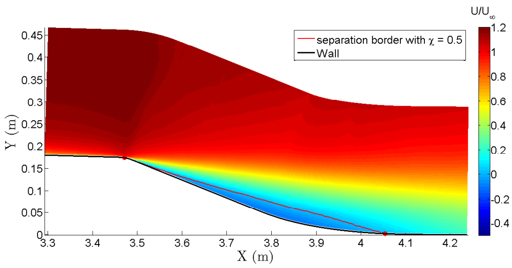

Figure 6. Mean streamwise velocity (U) on the flap at mid-span of the ramp.

In this reference frame the separation line can be detected. It was determined here using $\chi = 50\%$ criterion defined by Simpson (1989) and mentioned in introduction. The result is plotted in Figure 6. The separation border point for each mesh line at s was obtained by a linear interpolation between the first point from the wall where $\chi > 0.5$ and its following one with $\chi < 0.5$. To obtain a separation border detection below the first measurement point from the wall, the backflow coefficient at the wall (χ_w) was estimated by a linear extrapolation where there is at least two points from the wall having a χ greater than 30%. This extrapolation was based on the studies of Dengel & Fernholz (1990) and Lögdberg *et al.* (2010) who found that the backflow coefficient varies linearly very near the wall for $\chi > 0.3$.

In Figure 6, the separation and reattachment point positions are represented by a dot. The separation point is then located at $s = 3502$ mm compared to $s = 3500$ mm for the flap articulation. This position of the separation point is in close agreement with previous oil-film and wool-tufts visualisations results (Cuvier (2012)). The characteristics of the separation given by $\chi = 50\%$ can thus be considered as a reliable estimation. The reattachment point position is at $X = 4.05$ m. This leads to an attached flow development region downstream of the separation of about one δ_0 (with δ_0 the boundary layer thickness at $s = 3382$ mm) in the PIV field of view. The separation length (L_{sep}) is about 61 cm and the maximum height (H_{sep}) close to 3 cm. This leads to $\frac{H_{sep}}{H_{step}} = 0.17$ and $\frac{L_{sep}}{H_{step}} = 3.49$. Compared to the value obtained by Lin (1999) and Selby *et al.* (1992) for a similar configuration and momentum Reynolds number ($Re_\theta \simeq 9000$), the value $\frac{L_{sep}}{H_{step}}$ is about 3 times greater here. This is explained by a larger momentum thickness in this study, which was noticed by Simpson (1989) to increase $\frac{L_{sep}}{H_{step}}$ for a backward facing step.

Turbulence Intensities

Streamwise turbulence intensity

Figure 7 shows the streamwise turbulence intensity distribution $u = \sqrt{\overline{u'^2}}$ on the flap normalized by U_∞. Very high turbulent levels are observed originating at the separation point. This region develops downstream above the separation border and is generated by the shear due to separation. This peak of turbulence intensity in the external region is commonly observed in adverse pressure gradient and separated flows (Simpson (1989), Webster *et al.* (1996), etc.). The level of the peak is more than 2 times the level of the near wall region peak upstream of the separation. In the separation bubble, $\sqrt{\overline{u'^2}}$ is largely below the peak level, which is coherent with the observations of Simpson (1989) who shows that there is little turbulence production in the separated region.

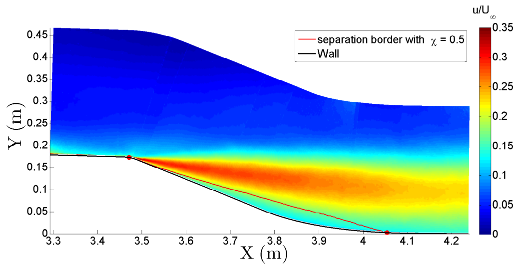

Figure 7. Streamwise turbulence intensity ($u = \sqrt{\overline{u'^2}}$) on the flap.

When looking at the instantaneous u-fluctuations, large coherent structures characterized by strong values of u' are observed in the region of high turbulence intensity. These structures can reach more than $3\delta_0$ in length and $0.5\delta_0$ in width, with δ_0 the upstream boundary layer thickness at $s = 3382$ mm. Their origin is at the flap articulation where the separation starts and could be linked to the high level of $\sqrt{\overline{u'^2}}$.

Figures 8 and 9 show respectively the distribution of $-\overline{u'v'}\frac{\partial U}{\partial y}$ and $-\overline{u'^2}\frac{\partial U}{\partial x}$ normalized by U_∞^3/H_{step}. These terms correspond to the accessible production terms of half the streamwise Reynolds stress ($\frac{1}{2}\overline{u'^2}$). Concerning the first one, upstream the flap, very close to the wall, high production levels are observed which correspond to the classical near wall turbulence production peak. However, the extends in wall-normal direction is largely higher than usual probably due to PIV uncertainty in the near wall region. In this region, the term $-\overline{u'^2}\frac{\partial U}{\partial x}$ (Figure 9) is negligible compared to the other term in Figure 8, which agrees with the standard approximations of 2D boundary layers (BL).

On the flap, in agreement with Simpson (1989), there is a strong streamwise Reynolds stress production region located above the separation border. It is dispatched into two distinct regions above the bubble : one in the first half of the separation and an other which starts near the middle of the separation and extends beyond the end of the PIV fields. The first region is characterized by high values of both production terms. However, these peak regions are not

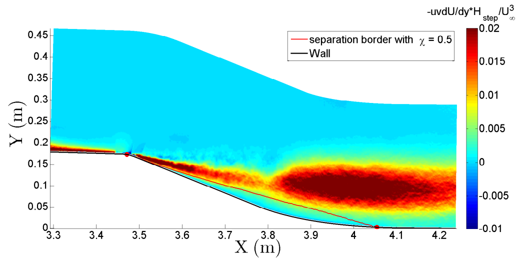

Figure 8. Production term $-\overline{u'v'}\frac{\partial U}{\partial y}$ of $\frac{1}{2}\overline{u'^2}$ on the flap.

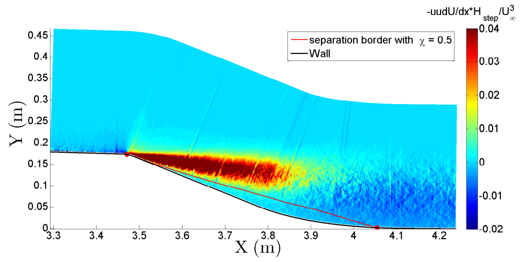

Figure 9. Production term $-\overline{u'^2}\frac{\partial U}{\partial x}$ of $\frac{1}{2}\overline{u'^2}$ on the flap.

at the same wall-normal distance. For $-\overline{u'v'}\frac{\partial U}{\partial y}$ it is less intense and closer to the wall. As a good superposition is observed in this region between the production term $-\overline{u'^2}\frac{\partial U}{\partial x}$ and $\sqrt{\overline{u'^2}}$ (Figure 7), it can be concluded that, along the first part of the flap, the streamwise turbulent intensity production is principally governed by $-\overline{u'^2}\frac{\partial U}{\partial x}$, which is itself cause by the strong deceleration generated by the sudden change in slope of the wall.

The downstream part of the separation is dominated by $-\overline{u'v'}\frac{\partial U}{\partial y}$ as for a 2D zero pressure gradient BL. It could be due to the change in wall direction near $X = 3.8$ m, which induces high levels of $\overline{v'^2}$ and $\overline{u'v'}$. Nevertheless, the second production region is highly linked to the separation as downstream of it, the production intensity decreases.

Wall-normal turbulence intensity

Figure 10 shows the wall-normal turbulence intensity distribution $v = \sqrt{\overline{v'^2}}$ on the flap normalized by U_∞. As for the streamwise component, high levels are observed in the external region above the separation bubble border. The origin is also at the separation point but the maximum is much more downstream than for the streamwise component and the peak is also wider in wall normal direction. Probably linked to the change in wall direction, after $X = 3.8$ m, the high level region is more intense and wider.

The accessible production terms for the wall-normal Reynolds stress $\frac{1}{2}\overline{v'^2}$ are $-\overline{u'v'}\frac{\partial V}{\partial x}$ and $-\overline{v'^2}\frac{\partial V}{\partial y}$. The first one was found negligible compared to the production terms of the streamwise component (more than 40 times lower). The second one is given in Figure 11. It is about 10 times lower but similar to the opposite of $-\overline{u'^2}\frac{\partial U}{\partial x}$ as expected from the 2D continuity equation and from the fact that $\overline{v'^2}$ is about 10 times lower than $\overline{u'^2}$ in this region. Globally, negative or negligible production is found for $\overline{v'^2}$ compared to $\overline{u'^2}$ in the whole field. But, looking at Figure 10, the level of this Reynolds stress increases with X. The redistribution term is the only one able to contribute to this increase. This is confirmed by a significant return toward isotropy in the rear

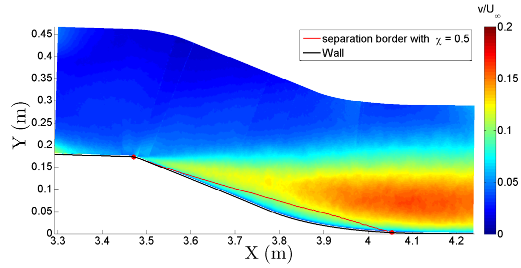

Figure 10. Wall normal turbulence intensity ($v = \sqrt{\overline{v'^2}}$) on the flap.

part of the field by comparing $\sqrt{\overline{u'^2}}$ and $\sqrt{\overline{v'^2}}$ in Figures 7 and 10. As the production of $\overline{v'^2}$ is negligible compared to the one of $\overline{u'^2}$, the turbulent kinetic energy production is then principally given by the production of the streamwise component.

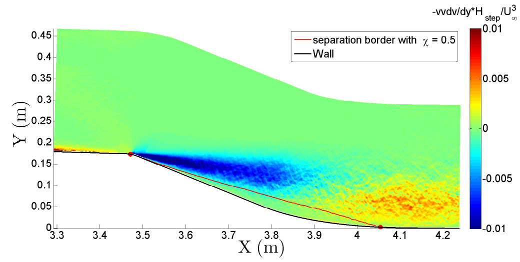

Figure 11. Production term $-\overline{v'^2}\frac{\partial V}{\partial y}$ of $\frac{1}{2}\overline{v'^2}$ on the flap.

Reynolds shear stress

Figure 12 shows the Reynolds shear stress distribution normalized by U_∞^2. The strong similarity between distributions of v and $-uv$ should be noted and also the fact that for both quantities, the peak develops in the rear part of the separation and downstream of it.

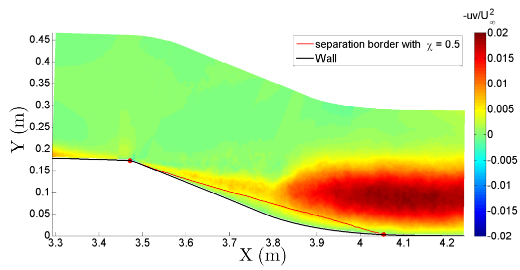

Figure 12. Reynolds shear stress ($uv = \overline{u'v'}$) on the flap.

Concerning the four production terms of the Reynolds shear stress accessible with the PIV set-up used, it was found that $\overline{v'^2}\frac{\partial U}{\partial y}$ largely dominates the three others. This term is then given in Figure 13 normalised by U_∞^3/H_{step}. The strong similarity between distributions of v and $-uv$ can then be explained by this term with produces Reynolds shear stress from the wall-normal Reynolds stress. This process is also found for boundary layers and it is also observed here upstream the of flap articulation.

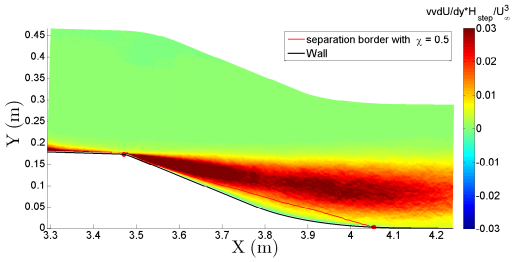

Figure 13. Production term $\overline{v'^2}\frac{\partial U}{\partial y}$ of $-\overline{u'v'}$ on the flap.

CONCLUSION

In this study, the flow separation induced by a flap of on two dimensional ramp has been characterized through streamwise 2D2C PIV measurement at mid-span. The field of view follows the wall surface and its size is about 28.7 cm in height above the wall and the curvilinear length is about 94 cm, so that it contains all the separation bubble and a part of the flow upstream and downstream of it. Four 2k*2k cameras where used to keep a relatively good spatial resolution with this very large field.

The separation border was detected with the backflow coefficient (Simpson (1989)) and it results that the separation length is about 61 cm ($\frac{L_{sep}}{H_{step}} = 3.49$) and the maximum height about 3 cm ($\frac{H_{sep}}{H_{step}} = 0.17$). The accessible turbulence intensity components with the PIV plane and their main production terms were also presented. The three Reynolds stresses ($\overline{u'^2}$, $\overline{v'^2}$, $\overline{u'v'}$) exhibit a region of very high level which develops above the separation border. This region for the streamwise Reynolds stress is found associated with very large scale structures characterized with high level of u'. The production of $\overline{u'^2}$ is found to dominate the production of turbulent kinetic energy which forces then a redistribution from $\overline{u'^2}$ to $\overline{v'^2}$ to explain the increase of the last one. The production term $\overline{u'^2}\frac{\partial U}{\partial x}$ drives the production of $\overline{u'^2}$ in the first part of the flap which is remarkable as it is not the case in zero pressure gradient boundary layers. Finally a high similarity is observed between $\overline{v'^2}$ and $\overline{u'v'}$ as the production of the last one is dominated by $\overline{v'^2}\frac{\partial U}{\partial y}$.

The results of this flow separation characterisation was used to highlight the modifications brought by applying active flow separation control with continuous jets vortex generators. The results are presented in an other paper.

ACKNOWLEGMENTS

The present research work was supported by International Campus on Safety and Intermodality in Transportation, the Nord-Pas-de-Calais Region, the European Community, the Regional Delegation for Research and Technology, the Ministry of Higher Education and Research, and the National Center for Scientific Research.

REFERENCES

Angele, K. P. 2003 Experimental studies of turbulent boundary layer separation and control. PhD thesis, Dept. Mechanics, Royal Institute of Technology, Stockholm.

Bradshaw, P. 1967 The response of a constant-pressure turbulent boundary layer to the sudden application of an adverse pressure gradient. *Tech. Rep.*. Royal Society, R. and M. No. 3575.

Carlier, J. & Stanislas, M. 2005 Experimental study of eddy structures in a turbulent boundary layer using particule image velocimetry. *J. Fluid Mech.* **535** (36), 143–188.

Chehroudi, B. & Simpson, R. L. 1985 Space-time results for a separating turbulent boundary layer using a rapidly scanning laser anemometer. *J. Fluid Mech.* **160**, 77–92.

Cuvier, C. 2012 Active control of a separated turbulent boundary layer in adverse pressure gradient. PhD thesis, Ecole Centrale de Lille.

Dengel, P. & Fernholz, H 1990 An experimental investigation of an incompressible turbulent boundary layer in the vicinity of separation. *J. Fluid Mech.* **212**, 615–636.

Foucaut, JM, Milliat, B., Perenne, N. & Stanislas, M. 2003 Characterisation of different piv algorithm using the europiv synthetic image generator and real images from a turbulent boundary layer. In *EUROPIV2 workshop, Zaragoza, Spain* (ed. Springer).

Herpin, Sophie, Wong, Chong Yau, Stanislas, Michel & Soria, Julio 2008 Stereoscopic piv measurements of a turbulent boundary layer with a large spatial dynamic range. *Exp Fluids* **45**, 745–763.

Kostas, J., Foucaut, J.-M & Stanislas, M. 2005 Application of double spiv on the near wall turbulence structure of an adverse pressure gradient turbulent boundary layer. In *6th International Symposium on PIV, Pasadena, CA*.

Lin, J. C. 1999 Control of turbulent boundary layer separation using micro-vortex generators. *AIAA Paper* (99-3404).

Lögdberg, Ola, Angele, Kristian & Alfredsson, Henrik 2010 On the robustness of separation control by streamwise vortices. *European Journal of Mechanics B/Fluids* **29**, 9–17.

Mellor, G. L. & Gibson, D. M. 1966 Equilibrium turbulent boundary layers. *J. Fluid Mech.* **24**, 225–253.

Selby, G. V., Lin, J. C. & Howard, F. G. 1992 Control of low-speed turbulent separated flow using jet vortex generators. *Experiments in Fluids* **12**, 394–400.

Simpson, R. L. 1989 Turbulent boundary layer separation. *Ann. Rev. Fluid Mech.* **21**, 205–234.

Simpson, R. L., Chew, Y.-T. & Shivaprasad, B. G. 1981*a* The structure of a separating turbulent boundary layer. part 1. mean flow and reynolds stresses. *J. Fluid Mech.* **113**, 23–51.

Simpson, R. L., Chew, Y.-T. & Shivaprasad, B. G. 1981*b* The structure of a separating turbulent boundary layer. part 2. higher-order turbulence results. *J. Fluid Mech.* **113**, 53–73.

Simpson, R. L., Strickland, J. H. & Barr, P. W. 1977 Features of a separating turbulent boundary layer in the vicinity of separation. *J. Fluid Mech.* **79**, 553–594.

Song, Simon, DeGraaff, David B. & Eaton, John K. 2000 Experimental study of a separating, reattaching, and redeveloping fow over a smoothly contoured ramp. *International Journal of Heat and Fluid Flow* **21**, 512–519.

Song, Simon & Eaton, John K. 2004 Flow structures of a separating, reattaching, and recovering boundary layer for a large range of reynolds number. *Experiments in Fluids* **36**, 642–653.

Webster, D. R., DeGraaff, D. B. & Eaton, J. K. 1996 Turbulence characteristics of a boundary layer on a two-dimensional bump. *J. Fluid Mech.* **320**, 53–69.